NIH Public Access
Author Manuscript
Bubble Sci Eng Technol. Author manuscript; available in PMC 2011 April 5.

Published in final edited form as:
Bubble Sci Eng Technol. 2010 December ; 2(2): 33–40.

Acoustic responses of monodisperse lipid-encapsulated microbubble contrast agents produced by flow focusing

Mehmet Kaya, Ph.D.,
University of North Carolina - North Carolina State University

Steven Feingold, B.S.,
University of North Carolina - North Carolina State University

Kanaka Hettiarachchi, Ph.D.,
University of California, Irvine

Abraham P Lee, Ph.D., and
University of California, Irvine

Paul A Dayton, Ph.D.*
UNC Chapel Hill and North Carolina State University

Abstract

Lipid-encapsulated microbubbles are used as contrast agents in ultrasound imaging. Currently available commercially made contrast agents have a polydisperse size distribution. It has been hypothesised that improved imaging sensitivity could be achieved with a uniform microbubble radius. We have recently developed microfluidics technology to produce contrast agents with a nearly monodisperse distribution. In this manuscript, we analyze echo responses from individual microbubbles from monodisperse populations in order to establish the relationship between scattered echo, microbubble radius, and excitation frequency. Simulations of bubble response from a modified Rayleigh-Plesset type model corroborate experimental data. Results indicate that microbubble echo response can be greatly increased by optimal combinations of microbubble radius and acoustic excitation frequency. These results may have a significant impact in the formulation of contrast agents to improve ultrasonic sensitivity.

Keywords

Ultrasound; microfluidics; size; molecular imaging; microbubble; contrast agent

INTRODUCTION

In the past, numerous efforts have been made to improve the sensitivity of ultrasound to blood flow. Possibly, the biggest accomplishment has been the introduction of contrast agents in the form of shell-stabilised, gas filled microbubbles. Due to the density and compressibility of their gas core, microbubbles scatter ultrasound waves much better than blood cells, and therefore can be utilised as intravascular contrast agents. Additionally, these compressible spheres oscillate nonlinearly in an acoustic field, allowing for the use of detection strategies which can separate microbubble signals from those of tissue.[1,2,3] Microbubbles have been proven to be effective diagnostic tools for ultrasound imaging as

*Corresponding author: padayton@bme.unc.edu.

NIH-PA Author Manuscript
NIH-PA Author Manuscript
NIH-PA Author Manuscript

NIH-PA Author Manuscript

NIH-PA Author Manuscript

NIH-PA Author Manuscript

well as for therapeutic applications such as targeted drug delivery, gene therapy and delivery, and sonothrombolysis.[4,5,6,7,8]

To date, microbubbles manufactured commercially for diagnostic or therapeutic purposes have consisted of populations that have large size variance (polydisperse). Typically, the polydisperse microbubbles are generated by sonication or mechanical agitation, resulting in a broad size distribution. Recently, there have been several groups striving to generate microbubble populations with low size variance. Ganan-Calvo and Gordillo were one of the first groups to report the usage of a flow-focusing device to produce monodisperse bubbles with a controllable diameter.[9] This work was extended to microfluidics by Garstecki, who demonstrated the production of micron-sized microbubbles as small as 5 microns with Polydimethylsiloxane (PDMS) systems.[10] Talu et al. and Hettiarachchi et al. have utilised both stainless steel and PDMS microfluidic flow-focusing devices, in conjunction with a surfactant/emulsifier mixture to achieve populations of stabilised monodisperse lipid-encapsulated microbubbles.[11,12] Additionally, Talu et al. demonstrated the correlation of acoustic responses of monodisperse encapsulated microbubbles produced by flow focusing as contrast agents for ultrasound imaging, as well as the ability to functionalise the surface for targeted imaging.[13] Recently, microfluidics technology has also been used to produce monodisperse micrometer-sized gas-filled lipospheres for chemotherapeutic drug delivery.[14] Pancholi and his colleagues used a T-junction device to prepare larger monodisperse microbubbles initially in the hundred-micron range; however, using a modified T-junction device they were able to generate phospholipid-coated air microbubbles with the smallest microbubbles having a mean diameter of 5.1±2 microns.[15,16] Another group has used ink-jet printing technology to generate gas-filled capsules with a polymeric shell and a diameter in the range of 5 microns.[17] Farook et al. have demonstrated co-axial electrohydrodynamic for the preparation of lipid-coated microbubble suspensions for a contrast agent population with a mean diameter of approximately 5 microns with a polydispersity index of about 9% under described conditions.[18,19] Recently, Feshitan et al. reduced the polydispersity of lipid-coated microbubbles using differential centrifugation; using this technique they were able to isolate the 1–2 and 4–5 microns microbubble diameter fractions.[20]

The motivation behind producing microbubbles with a narrow size distribution is several fold. Nearly all interactions of an ultrasound wave with microbubbles depend on the microbubble size. Parameters such as the destruction threshold, the amount of radiation force experienced, and the resonant frequency, are all affected by microbubble radius (Figure 1).[21,22,23] For vehicles in the 0.5–10 micron range, which is the most common range for intravascular microbubbles,[24] all of these parameters change drastically with small differences in diameter. Thus, motivation is strong for utilising uniformly sized bubbles in order to have a consistent response from the entire microbubble population.

The use of monodisperse microbubbles becomes particularly important with molecular imaging. Molecular imaging with ultrasound entails microbubbles coated with adhesion ligands that bind to receptors on cells at sites of angiogenesis, inflammation or thrombus.[25,26,27,28,29] The ligands for this purpose can be antibodies, peptides or peptidomimetrics that are specific to molecular markers of a given pathology.[30,31] For non-targeted blood pool imaging, approximately 10^8 to 10^{10} polydisperse microbubbles are injected intravascularly, and this large number of circulating contrast agents alleviates the need to be very sensitive to small numbers of agents. However, it has been observed that for targeted molecular imaging, only a limited number of ligand attached microbubbles are retained at the site of pathology,[32,5,26,29] therefore increasing the need for improved ultrasound imaging sensitivity to small numbers of contrast agents.

NIH-PA Author Manuscript

NIH-PA Author Manuscript

NIH-PA Author Manuscript

In this manuscript, we focus on the relationship of microbubble size to imaging parameters such as the scattered echo and the resonant frequency. Talu et al. had previously postulated that a mechanism of sensitivity of ultrasound to microbubbles would be to match the microbubble resonant frequency to the transducer center frequency.[13] Since the resonant frequency of a microbubble is inversely related to its size, a more monodisperse population of microbubbles with a resonance frequency distribution overlapping the imaging bandwidth could result in an intensified echo amplitude, hence in an improved ultrasound image. Although in the previous study by Talu et al., preliminary acoustic results showed that the echoes received from monodisperse microbubbles are significantly more correlated compared to the echoes received from polydisperse microbubbles,[13] at the time the investigators were not able to experimentally assess the amplitude response as a function of size and interrogation frequency.

Aside from the preliminary data previously presented by Talu et al,[13] the acoustic response from individual monodisperse lipid-encapsulated microbbubles in the diameter range relevant for ultrasound imaging has not yet been thoroughly investigated. In this study, we present simulations and experimental acoustic results from individual monodisperse microbubbles that are generated using a flow-focusing microfluidic system. The echo characteristics of monodisperse microbubbles are evaluated both experimentally and with simulations at varying excitation frequencies. Acoustic response amplitude is compared for simulated populations of monodisperse and polydisperse microbubbles.

MATERIALS AND METHODS

Simulations

There are many models available in the literature proposed for simulating radial oscillation of microbubbles in response to acoustic pulses, including those by Marmottant, Doinikov, Chatterjee, and Hoff, to name a few examples.[33,34,35,36] Our simulations used the model validated by Zheng et al. to estimate microbubble oscillation in response to an acoustic pulse.[37] Zheng demonstrated excellent agreement between simulations and experimentally recorded radius-time curves (through ultra high-speed imaging) of sonicated lipid-shelled microbubbles, similar to those studied in this manuscript.[37] This model uses a modified Raleigh-Plesset equation to simulate the radial dynamics of the contrast agents and accounts for shell properties and radiation damping.

To predict the acoustic response from the bubbles based on the radial oscillation calculated from the model, a simplified relationship among the time-dependent radius, wall velocity, acceleration and scattered pressure is used.[38]

$$\varphi = -R^2\dot{R}\,r^{-1} \tag{1}$$

$$P = -\rho\,\dot{\varphi} = \rho r^{-1}(R^2\ddot{R} + R\,\dot{R}^2) \tag{2}$$

where

φ = velocity potential

R = instantaneous bubble radius

$\dot{R}$ = wall velocity of bubble

NIH-PA Author Manuscript

NIH-PA Author Manuscript

NIH-PA Author Manuscript

$\ddot{R}$ = acceleration of bubble wall

P = scattered acoustic pressure

r = distance from bubble

Since polydisperse microbubbles with carefully controlled mean diameters are not experimentally available, we simulated acoustic responses from polydisperse populations of bubbles in order to compare polydisperse populations with monodisperse populations. The simulated polydisperse distribution followed a Gaussian curve with standard deviation of 0.3 μm in bubble radius. This distribution shape was chosen to resemble an experimental population with center radius of 0.5 microns sorted via centrifugation as previously reported.[39] The mean of the distribution was linearly shifted across the range of radii simulated, while maintaining the standard deviation of 0.3 μm. Bubbles in the polydisperse populations larger than 7 μm were eliminated to replicate filtering effects from capillaries as might be seen in the microvasculature. Excitation was modeled over a range of frequencies between 1 and 10 MHz and mean radii between 0.5 and 3.5 μm. The percent difference between the echoes from the monodisperse and polydisperse populations was taken at each frequency and matching mean radius. Echo responses were calculated from matched concentrations between the two populations. Simulations involved 60 size bins (the number of size bins read from our Accusizer 780 particle sizer), and a total of approximately 30,000 bubbles per distribution.

Experimental System

Microbubble formation

Monodisperse contrast agents were produced using a microfluidic flow focusing as previously described.[12,11,13] Briefly, poly-dimethyl siloxane (PDMS) was used to mold a flow focusing chamber with an orifice diameter of 10 micron and gas and liquid channel widths of 35 and 50 microns respectively. The channels were filled with distilled water immediately after mounting the PDMS to the glass microscope slide base to ensure the hydrophilic character of the walls of microchannels. A calibrated syringe pump (Harvard Apparatus, Holliston, MA) was used to pump liquid reagents through the chamber. Nitrogen gas was provided through a low-pressure regulator (Sub-miniature precision regulator, Airtrol Inc., WI, USA) from a compressed gas cylinder. By adjusting the liquid and gas flow rates, the mean radius of the microbubbles produced could be precisely controlled.

Microbubble Formulation

The lipid solution for producing microbubbles was prepared as described.[11] The lipids 1,2-distearoyl-sn-glycero-3-phosphocholine (DSPC) and 1,2-distearoyl-sn-glycero-3-phosphoethanolamine-N-[methoxy(polyethylene glycol) 2000] (DSPE-PEG2000) were purchased from Avanti Polar Lipids (Alabaster, AL, USA). The lipids were dissolved in a solution of 98 vol % deionised water with 1 vol % glycerol, 92 g/mol (Fisher Scientific, Pittsburgh, PA) and 1 vol % propylene glycol, 76 g/mol (Sigma-Aldrich, St. Louis, MO, USA) added for viscosity control. The lipid composition utilised a 9:1 mol:mol ratio of DSPC to DSPE-PEG2000.

The lipids dissolved in chloroform were dried under nitrogen and degassed in the oven at 60 degrees Celsius for half an hour to evaporate the solvent. Once the lipids were dry, the buffer solution was added to the lipids in a vial. The lipid solution was sonicated until a transparent and homogeneous mixture was achieved.

NIH-PA Author Manuscript

NIH-PA Author Manuscript

NIH-PA Author Manuscript

Optical visualization

The flow focusing chamber was mounted on a custom stage system on an Olympus IX-71 (Olympus, Tokyo, Japan) inverted microscope. Monodisperse microbubbles exiting the flow focusing chamber (Figure 2a) were pumped through a 200 micrometer inner diameter cellulose tube (Spectrum Laboratories, Rancho Dominguez, CA, USA) which was positioned in a water bath for acoustic measurements and also within the field of view of the microscope objective (20X LCPlanFI, Olympus, Tokyo, Japan) (Figure 2b). A high-speed camera (APS-RX, Photron, Inc., San Diego, CA) operating at a frame rate of 5,000 FPS with a 1/50,000 shutter speed coupled to the microscope was required to image the individual microbubbles traveling through the narrow field of view. Optical frame captures of bubble radius were acquired during acoustic data acquisition. Video calibration was performed using a scale reticle (Edmund Optics, NJ, USA), and data were analyzed offline using Photoshop CS3 software (Adobe Systems Inc., San Jose, CA, USA).

Acoustic sampling

The acoustic responses of microbubbles as a function of radius were acquired using a custom pulse-echo acoustic system integrated with the microscope, high speed camera, and microfluidics system (Figure 2c). A 3-axis positioning system mounted on the microscope was used to align the ultrasonic transducer assembly with the cellulose tube so that microbubbles could be acoustically interrogated. Total distance from the exit orifice of the flow focusing chamber to the optical and acoustical sample volumes was less than 5 cm, and hence microbubbles were optically and acoustically interrogated almost immediately after production.

A single element ultrasound transducer with a nominal center frequency of 0.93 MHz and 6dB bandwidth of 0.56–1.27 MHz (Valpey Fisher Corp., Hopkinton, MA, USA) was used for transmission. Transducer excitation voltage was provided by an arbitrary waveform generator (AWG 2021, Tektronix, Inc., Beaverton, OR, USA) and amplified with a RF amplifier (3200L, ENI, Rochester, NY, USA). In order to sample each microbubble with a range of frequencies, the pulse sequence consisted of a train of five cycle pulses each with a different frequency (0.75, 1.25, 1.75, 2.5 and 3.0 MHz). A calibrated needle hydrophone (HNZ-0400, Onda Corp., Sunnyvale, CA, USA) was used for calibration of the acoustic system. Based on the calibration, transducer excitation voltage was adjusted so that pulses of each frequency had the same pressure amplitude despite the frequency response of the transducer. The excitation pulses were separated by 5 microseconds, each producing 100 kPa of peak negative pressure. The receiver transducer had a nominal center frequency of 2.2 MHz with a −6dB bandwidth of 1.36–3.04 MHz. (Olympus/Panametrics, Waltham MA, USA). Acoustic data were amplified by 40 dB and band-pass filtered between 1 and 12 MHz with a receiver (BR-640, Ritec, Warwick, RI, USA), then digitised at 100 MHz sample rate with 14 bit A/D resolution by a data acquisition signal waveform digitiser (PDA14, Signatec Inc., CA, USA) through a LabView (National Instruments Corp., Austin, TX) interface. The echoes from ultrasound driven microbubbles were captured in M-mode, and 50 echoes for each microbubble size were analyzed offline in MATLAB (The Mathworks Inc, Natick, MA, USA).

RESULTS

We were able to produce nearly monodisperse microbubbles in the radii range of 1.8–4.8 microns with a single microfluidics chamber by varying the gas inlet pressure and the fluid flow rate. Typical production rates were on the order of 10–100 microbubbles/second depending on the flow parameters. For each monodisperse microbubble size, at least 10 optical images were captured and analyzed to calculate the mean radius and standard

NIH-PA Author Manuscript

NIH-PA Author Manuscript

NIH-PA Author Manuscript

deviation of the microbubbles. With this system, it was not possible to capture the optical diameter for the exact microbubble for which we recorded the acoustic response, however, the benefit of the monodisperse production insured that optically measured diameters were representative of the population. Monodispersity was on the order of ±0.1 micron for the smallest bubbles measured (1.8 microns), and ± 0.2 micron for the largest bubbles measured (4.8 microns). Because of the relatively slow production rates, we were able to acquire echo signatures from one bubble at a time.

Ultrasound excitation frequencies of 0.75 MHz – 3.0 MHz were utilised to excite microbubbles with radii optically measured to be between 1.8 and 4.8 microns. Experimentally recorded echoes from uniformly-sized microbubbles produced by the chamber were in agreement with simulations (Figure 3).

Analysis of experimental results for the monodisperse microbubbles demonstrated that the amplitude of the scattered echo received was always larger for the frequency closest to bubble resonance (illustrated by an asterisk over the corresponding amplitude bar) compared with frequencies farthest from resonance within the range tested (Figure 3a). For microbubbles with a radius of 4.8 microns, amplitude of the echo received closest to the resonance frequency (0.011 volts at 0.75 MHz) was approximately 8.4 times larger than the echo amplitude acquired farthest from the resonance frequency (0.0013 volts at 3 MHz).

Amplitude of the scattered echo was also observed to increase as a function of bubble radius. The strongest scattered echo amplitude was received using the largest microbubbles tested, which had a radius of 4.8 microns (0.011 volts at 0.75 MHz). The amplitude of echoes from these bubbles was approximately 5.3 times larger than the echo amplitude received (0.002 volts at 1.75 MHz) from the smallest microbubbles tested (a radius of 1.8 microns), when each was excited with a frequency closest to their resonant frequency. The largest echo amplitude obtained using microbubbles with a radius of 3 microns (0.007 volts at 1.25 MHz) was approximately 3.5 times higher than the echo received with the smallest monodisperse microbubbles. Simulations were in good agreement with experimental data (Figure 3(b)).

Due to the challenge of producing approximately 0.5 micron radius monodisperse agents with our experimental system, we considered these smaller microbubbles only with simulations. Additionally, we expanded the frequency range up to 15 MHz. Simulations demonstrated that for microbubbles with a radius of 0.75 micron, 1.5 microns, and 3.0 microns, optimal echo signal would be achieved if microbubbles were excited at 6.5 MHz, 2.8 MHz, and 1.1 MHz, correlating with resonance frequencies for these agents of 5.8 MHz, 2.5 MHz, and 1.1 MHz correspondingly (Figure 4). If the center frequency was held constant, optimal echo signature was estimated to occur with the largest microbubble (Figure 5).

Simulated acoustic responses from polydisperse populations of bubbles were compared with those from monodisperse bubbles in order to compare the acoustic response from these different population types. Excitation was modeled over a range of frequencies between 1 and 10 MHz. The percent difference between the echoes from the monodisperse and polydisperse populations was taken at each frequency and matching mean radius (Figure 6).

Simulations demonstrated that for transmitted pulses near the resonant frequency of the mean bubble radius, a monodisperse population would produce echoes between 15% to 60% stronger than a polydisperse population. At frequencies higher than the resonance frequency, the monodisperse distributions were slightly more echogenic (approximately 5%) than the polydisperse populations. Below resonance frequency, polydisperse populations performed much better (25% to 170%). At these frequencies, the large bubbles in the tails of the

NIH-PA Author Manuscript

NIH-PA Author Manuscript

NIH-PA Author Manuscript

polydisperse distribution were being excited close to their resonant frequency and hence contributed significantly to the response.

DISCUSSSION

By using microfluidic flow-focusing technology, we were consistently able to generate monodisperse microbubbles with a very narrow size distribution. Besides its simplicity and low-cost, one of the biggest advantages of using a microfluidic flow-focusing device is the ability to produce a monodisperse distribution, and the ability to readily change the mean size of microbubbles produced. One limitation was that our microfluidic system was unable to produce microbubbles with a radius on the order of a micron or smaller. To be able to achieve this goal, it is likely that the channel depth and the orifice size of the microfluidic flow focusing device would need to be reduced.

The primary challenge with our microfluidic technology is the low production rate when generating small microbubbles, which was several orders of magnitude less than that achieved by mechanical agitation or sonication methods. One method to overcome the low production rate challenge is multiplexing microfluidics devices; however, the production rate per chip would also need to be increased to make this a feasible production method even for small animal imaging studies. Nevertheless, the flow focusing technology demonstrated to be a controlled way of precisely producing microbubbles of controlled diameter for acoustic analysis.

Through ultrasound experiments supported with optical visualization, we analysed the effect of monodispersity and size of lipid-encapsulated microbubble contrast agents on the scattered ultrasound echo. In addition, we investigated means to achieve optimal acoustic response that is based on the relationship between resonant frequency of microbubbles and transducer center frequency used for transmission. Our experimental results were in fairly good agreement with simulations (Table 1), although experimental data did not illustrate the larger acoustic response for bubbles in the 3.9–4.4 micron range compared to the 3–3.5 micron range, as was predicted by simulations. We hypothesize that this was due to experimental error in correlating bubble size with acoustic response. Occasionally, a few larger or smaller microbubbles were interspersed with the main monodisperse stream due to momentary discrepancies in the flow, and these outliers could readily bias the mean acoustic response. We tried to avoid acquiring data when this occurred, but it was not possible to monitor bubble size at all times, as the high speed camera acquired for intervals of only 2 seconds.

Two factors were shown to allow the user to optimise echo response from microbubbles. First, the size of an ultrasound-driven microbubble was proportional to amplitude of the scattered echo when excited off resonance; larger microbubbles produced louder echoes (Table 1). Second, maximum acoustic response was received when a microbubble was excited at its resonant frequency.

Our simulations demonstrated that depending on the relationship of the imaging frequency to the bubble population mean diameter, either a polydisperse or monodisperse population could result in the best imaging sensitivity. In cases where the imaging frequency was lower than the mean resonant frequency of the bubble population, the polydisperse population was estimated to produce a significantly better response than the monodisperse population. This was largely due to the fact that the largest bubbles provided the most substantial response, even when excited off-resonance, compared to smaller bubbles excited on-resonance. If the mean resonant frequency of the bubble population was similar to the imaging frequency, the monodisperse population produced the highest signal amplitude. There was a minor benefit in acoustic response from the monodisperse population for imaging frequencies greater than

NIH-PA Author Manuscript

NIH-PA Author Manuscript

NIH-PA Author Manuscript

the mean resonance frequency. The benefits of on-resonance excitation with a monodisperse population were greatest for smaller bubbles. This result is explained by the steep slope of the resonance frequency curve at small bubble radii. Since a small change in bubble radius causes a large change in resonant frequency, only a small percentage of bubbles in a polydisperse population will be excited near resonant frequency for bubbles in this size range.

Conclusion

Through ultrasound experiments supported with optical visualization and with simulations, we assessed the acoustic response of lipid-encapsulated monodisperse microbubbles of different in response to various excitation frequencies. Simulations of echo response using models of bubble oscillation were shown to be in good agreement with experimentally measured responses. We observed that when excited near resonance, the acoustic response of monodisperse microbubbles increased with microbubble radius. Additionally, microbubbles with a larger radius were more echogenic than smaller microbubbles. Thus, it is possible to substantially increase the sensitivity of an ultrasound imaging system to microbubble contrast agents by decreasing the polydispersity of the contrast agent distribution, by exciting microbubbles near resonance, and by using larger microbubbles given a constant concentration. These results may have a significant impact in situations where maximum detection sensitivity is needed to small concentrations of contrast agents, such as in ultrasonic molecular imaging.

Acknowledgments

These studies were supported by the NIH Roadmap for Medical Research, grant R21EB005325 and in part by R03EB006846. We appreciate the contributions of Drs. Shukui Zhao, Esra Talu, and Marjorie Longo in preliminary studies. This manuscript is based on pilot studies that were presented and published in the conference proceedings of the 2009 IEEE Ultrasonics Symposium (copyright IEEE).

REFERENCE LIST

1. Sboros V. Response of contrast agents to ultrasound. Advanced drug delivery reviews. 2008; 60:1117–36. [PubMed: 18486270]
2. Burns PN, Wilson SR. Microbubble contrast for radiological imaging: 1. Principles Ultrasound quarterly. 2006; 22:5–13.
3. Dayton PA, Rychak JJ. Molecular ultrasound imaging using microbubble contrast agents. Front Biosci. 2007; 12:5124–42. [PubMed: 17569635]
4. Dayton PA, Ferrara KW. Targeted imaging using ultrasound. J Magn Reson Imaging. 2002; 16(4): 362–77. [PubMed: 12353252]
5. Klibanov AL. Microbubble contrast agents - Targeted ultrasound imaging and ultrasound-assisted drug-delivery applications. Investigative Radiology. 2006; 41(3):354–62. [PubMed: 16481920]
6. Lindner JR, Kaul S. Delivery of drugs with ultrasound. Echocardiography. 2001; 18(4):329–37. [PubMed: 11415506]
7. Villanueva FS. Molecular imaging of cardiovascular disease using ultrasound. J Nucl Cardiol. 2008; 15(4):576–86. [PubMed: 18674725]
8. Unger EC, Matsunaga TO, McCreery T, Schumann P, Sweitzer R, Quigley R. Therapeutic applications of microbubbles. Eur J Radiol. 2002 May; 42(2):160–8. [PubMed: 11976013]
9. Gañán-Calvo AM, Gordillo JM. Perfectly monodisperse microbubbling by capillary flow focusing. Phys Rev Lett. 2001; 87(27 Pt 1):274501. [PubMed: 11800883]
10. Garstecki P, Ganan-Calvo AM, Whitesides GM. Formation of bubbles and droplets in microfluidic systems. Bull Pol Acad Sci Tech Sci. 2005; 53:361–72.

NIH-PA Author Manuscript

NIH-PA Author Manuscript

NIH-PA Author Manuscript

11. Talu E, Lozano MM, Powell RL, Dayton PA, Longo ML. Long-term stability by lipid coating monodisperse microbubbles formed by a flow-focusing device. Langmuir. 2006; 22(23):9487–90. [PubMed: 17073468]
12. Hettiarachchi K, Talu E, Longo ML, Dayton PA, Lee AP. On-chip generation of microbubbles as a practical technology for manufacturing contrast agents for ultrasonic imaging. Lab Chip. 2007; 7(4):463–8. [PubMed: 17389962]
13. Talu E, Hettiarachchi K, Zhao S, Powell RL, Lee AP, Longo ML, Dayton PA. Tailoring the size distribution of ultrasound contrast agents: possible method for improving sensitivity in molecular imaging. Mol Imaging. 2007; 6(6):384–92. [PubMed: 18053409]
14. Hettiarachchi K, Zhang S, Feingold S, Lee AP, Dayton PA. Controllable microfluidic synthesis of multiphase drug-carrying lipospheres for site-targeted therapy. Biotechnol Prog. 2009 Jul–Aug; 25(4):938–45. [PubMed: 19455647]
15. Pancholi KP, Farook U, Moaleji R, Stride E, Edirisinghe MJ. Novel methods for preparing phospholipid coated microbubbles. Eur Biophys J. 2008; 37(4):515–20. [PubMed: 17687548]
16. Pancholi K, Stride E, Edirisinghe M. Generation of microbubbles for diagnostic and therapeutic applications using a novel device. J Drug Target. 2008; 16(6):494–501. [PubMed: 18604662]
17. Böhmer MR, Schroedersa R, Steenbakkersa JAN, de Wintera SHPM, Duinevelda PA, Luba J, Nijssena WPM, Pikkemaata JA, Staperta HR. Preparation of monodisperse polymer particles and capsules by ink-jet printing. Colloids and Surfaces A: Physicochemical and Engineering Aspects. 2006 October; 289(1–3):96–104.
18. Farook U, Stride E, Edirisinghe MJ. Preparation of suspensions of phospholipid-coated microbubbles by coaxial electrohydrodynamic atomization. J R Soc Interface. 2009; 6(32):271–7. [PubMed: 18647738]
19. Farook U, Stride E, Edirisinghe MJ. Controlling size and size distribution of electrohydrodynamically prepared microbubbles. Bubble Science, Engineering & Technology. 2009 November; 1(1–2):53–57.
20. Feshitan Jameel A, Chen Cherry C, Kwan James J, Borden Mark A. Microbubble size isolation by differential centrifugation. Journal of Colloid and Interface Science. 2009; 329:316–324. [PubMed: 18950786]
21. Chomas JE, Dayton P, May D, Ferrara K. Threshold of fragmentation for ultrasonic contrast agents. J Biomed Opt. 2001; 6(2):141–50. [PubMed: 11375723]
22. Morgan KE, Allen JS, Dayton PA, Chomas JE, Klibanov AL, Ferrara KW. Experimental and theoretical evaluation of microbubble behavior: effect of transmitted phase and bubble size. IEEE Trans Ultrason Ferroelectr Freq Control. 2000; 47(6):1494–509. [PubMed: 18238696]
23. Dayton PA, Allen JS, Ferrara KW. The magnitude of radiation force on ultrasound contrast agents. J Acoust Soc Am. 2002 Nov; 112(5 Pt 1):2183–92. [PubMed: 12430830]
24. Sirsi SR, Borden MA. Microbubble compositions, properties and biomedical applications. Bubble Sci, Eng & Technology. 2009; 1(1):3–17.
25. Dayton PA, Pearson D, Clark J, Simon S, Schumann PA, Zutshi R, Matsunaga TO, Ferrara KW. Ultrasonic analysis of peptide- and antibody-targeted microbubble contrast agents for molecular imaging of alphavbeta3-expressing cells. Mol Imaging. 2004 Apr; 3(2):125–34. [PubMed: 15296677]
26. Leong-Poi H, Christiansen J, Klibanov AL, Kaul S, Lindner JR. Noninvasive assessment of angiogenesis by ultrasound and microbubbles targeted to alpha(v)-integrins. Circulation. 2003 Jan 28; 107(3):455–60. [PubMed: 12551871]
27. Lindner JR, Song J, Xu F, Klibanov AL, Singbartl K, Ley K, Kaul S. Noninvasive ultrasound imaging of inflammation using microbubbles targeted to activated leukocytes. Circulation. 2000 Nov 28; 102(22):2745–50. [PubMed: 11094042]
28. Rychak JJ, Lindner JR, Ley K, Klibanov AL. Deformable gas-filled microbubbles targeted to P-selectin. J Control Release. 2006 Sep 12; 114(3):288–99. [PubMed: 16887229]
29. Schumann PA, Christiansen JP, Quigley RM, McCreery TP, Sweitzer RH, Unger EC, Lindner JR, Matsunaga TO. Targeted-microbubble binding selectively to GPIIb IIIa receptors of platelet thrombi. Invest Radiol. 2002 Nov; 37(11):587–93. [PubMed: 12393970]

NIH-PA Author Manuscript

NIH-PA Author Manuscript

NIH-PA Author Manuscript

30. Behm CZ, Lindner JR. Cellular and molecular imaging with targeted contrast ultrasound. Ultrasound Q. 2006 Mar; 22(1):67–72. [PubMed: 16641795]

31. Lanza GM, Wickline SA. Targeted ultrasonic contrast agents for molecular imaging and therapy. Curr Probl Cardiol. 2003 Dec; 28(12):625–53. [PubMed: 14691443]

32. Ellegala DB, Leong-Poi H, Carpenter JE, Klibanov AL, Kaul S, Shaffrey ME, Sklenar J, Lindner JR. Imaging tumor angiogenesis with contrast ultrasound and microbubbles targeted to alpha(v)beta3. Circulation. 2003 Jul 22; 108(3):336–41. [PubMed: 12835208]

33. Marmottant P, Sander van der Meer, Emmer M, Versluis M, de Jong N, Hilgenfeldt S, Lohse D. A model for large amplitude oscillations of coated bubbles accounting for buckling and rupture. J Acoust Soc Am. 2005; 118 (6):3499–3505.

34. Doinikov AA, Dayton PA. Maxwell rheological model for lipid-shelled ultrasound microbubble contrast agents. J Acoust Soc Am. 2007 Jun; 121(6):3331–40. [PubMed: 17552685]

35. Chatterjee D, Sarkar K. A Newtonian rheological model for the interface of microbubble contrast agents. Ultrasound Med Biol. 2003 Dec; 29(12):1749–57. [PubMed: 14698342]

36. Hoff L, Sontum PC, Hovem JM. Oscillations of polymeric microbubbles: effect of the encapsulating shell. J Acoust Soc Am. 2000 Apr; 107(4):2272–80. [PubMed: 10790053]

37. Zheng H, Dayton PA, Caskey C, Zhao S, Qin S, Ferrara KW. Ultrasound-driven microbubble oscillation and translation within small phantom vessels. Ultrasound Med Biol. 2007 Dec; 33(12): 1978–87. [PubMed: 17900793]

38. Morgan KE, Allen JS, Chomas JE, Dayton PA, Ferrara KW. Experimental and Theoretical Analysis of Individual Contrast Agent Behavior. Proc IEEE Ultras Symposium. 1999:1685–88.

39. Streeter J, Gessner R, Miles I, Dayton PA. Improving Sensitivity in Ultrasound Molecular Imaging By Tailoring Contrast Agent Size Distribution: In Vivo Studies. Mol Imaging. 2010 Apr; 9(2):87–95. [PubMed: 20236606]

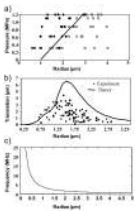

Figure 1.
Microbubble parameters as a function of radius as previously described. (a) Destruction threshold at 2.25 MHz (b) radiation force at 2.25 MHz, and (c) resonant frequency. Reproduced with permission from: [21] (copyright 2002, Acoustical Society of America), and [23] (copyright 2001, SPIE).

NIH-PA Author Manuscript NIH-PA Author Manuscript NIH-PA Author Manuscript

NIH-PA Author Manuscript

NIH-PA Author Manuscript

NIH-PA Author Manuscript

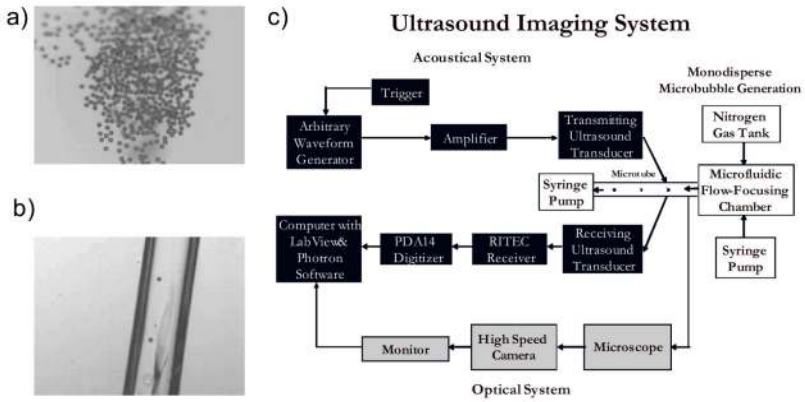

Figure 2.

(a) Images of monodisperse microbubbles produced from the microfluidic chamber exiting the orifice and (b) being pumped down a 200 micron cellulose tube for acoustic interrogation. (c) Diagram of the experimental system.

NIH-PA Author Manuscript

NIH-PA Author Manuscript

NIH-PA Author Manuscript

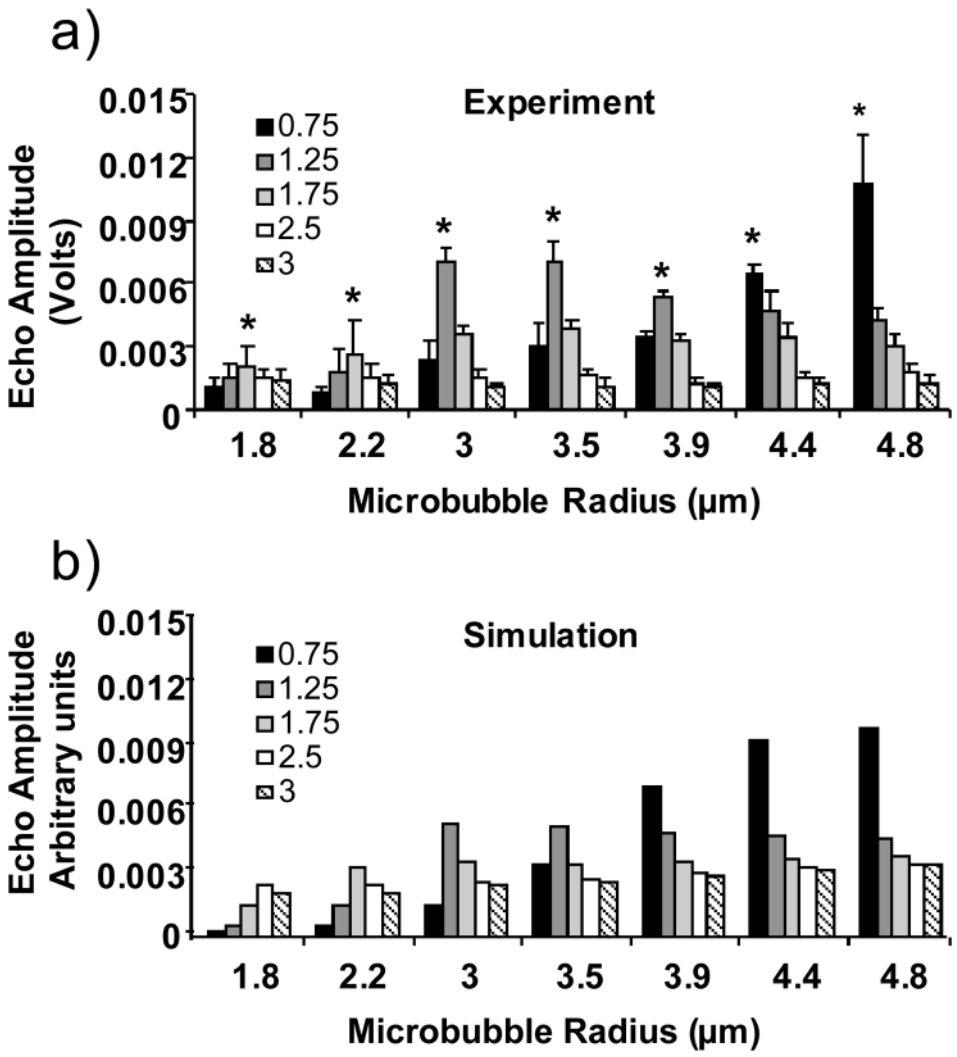

Figure 3.

Amplitude of echo responses of monodisperse microbubbles with respect to microbubble radii and excitation frequencies (a) Experimental Results. Asterisks (*) correspond to the excitation frequency that is closest to the resonant frequency for the given monodisperse microbubble radius (b) Simulation results with the same range of monodisperse microbubble radii.

NIH-PA Author Manuscript

NIH-PA Author Manuscript

NIH-PA Author Manuscript

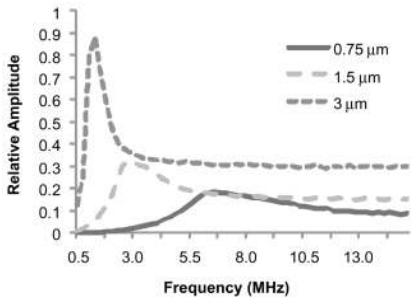

Figure 4.
Simulation of echo amplitudes from monodisperse microbubbles as a function of excitation frequency for 3 bubble radii: 0.75, 1.5 and 3 µm.

NIH-PA Author Manuscript

NIH-PA Author Manuscript

NIH-PA Author Manuscript

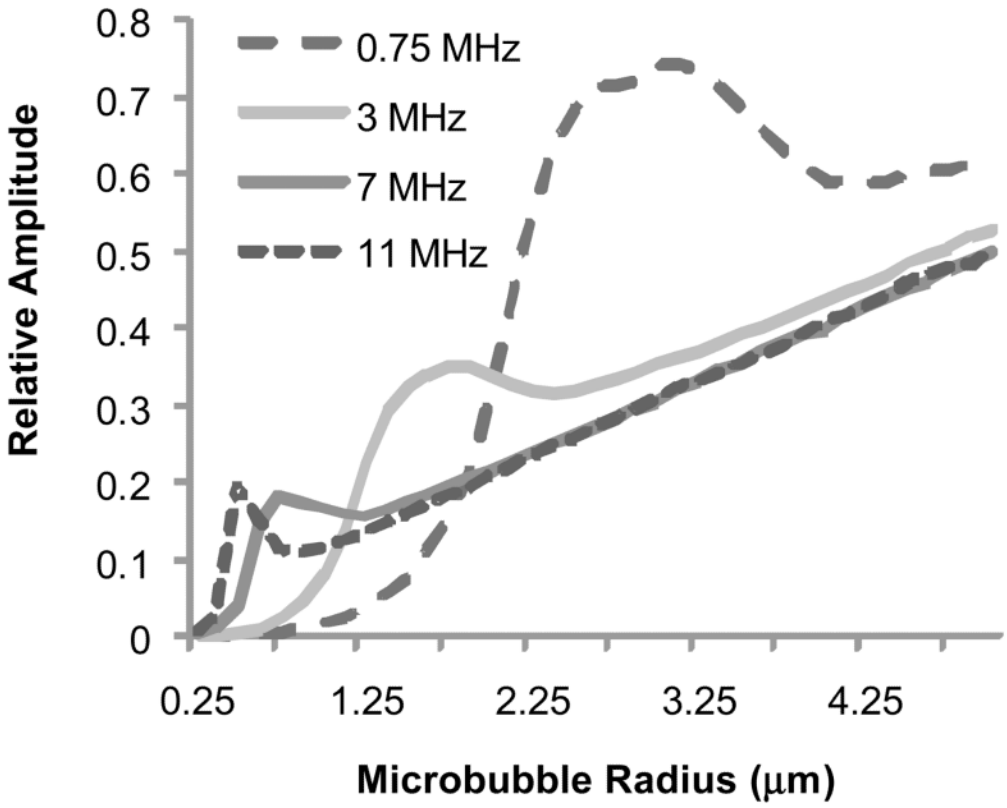

Figure 5.
Simulation of echo amplitudes from monodisperse microbubbles as a function of radius for 4 excitation frequencies: 0.75, 3, 7 and 11 MHz.

NIH-PA Author Manuscript

NIH-PA Author Manuscript

NIH-PA Author Manuscript

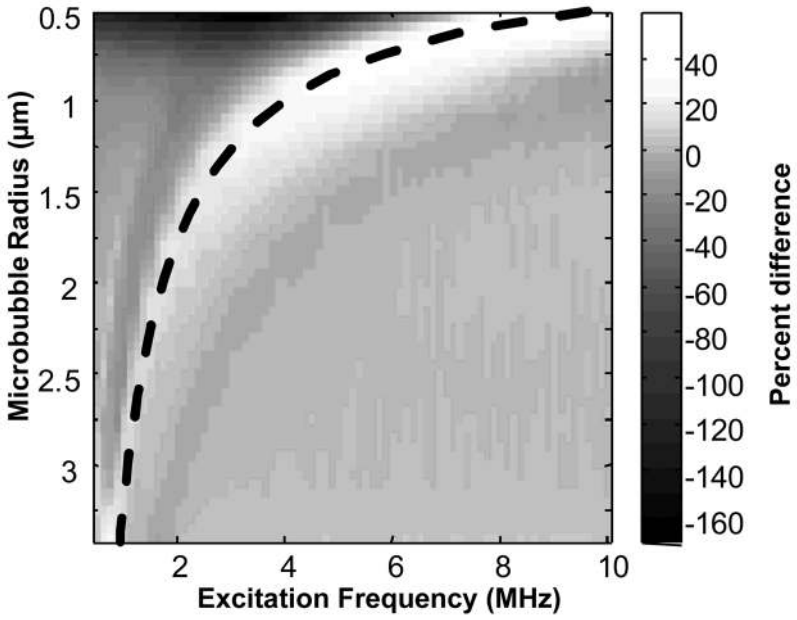

Figure 6.
The percent difference between the echo amplitudes from monodisperse and polydisperse populations computed at excitation frequencies between 1–10 MHz for populations with mean radii ranging from 0.5 to 3.5 microns. Dotted line represents resonant frequency range.

NIH-PA Author Manuscript

NIH-PA Author Manuscript

NIH-PA Author Manuscript

Table 1

Comparison of amplitude of responses for bubbles of varying radius when excited with optimal frequency (within the range tested), determined by experiment and simulation.

Bubble Radius (μm)	Ratio between maximal response and maximum response of 1.8 μm bubble (experimental)	Ratio between maximal response and maximum response of 1.8 μm bubble (simulations)	Percent difference between experimental and simulation
4.8	5.27	4.39	17
4.4	3.15	4.19	−33
3.9	2.65	3.31	−24
3.5	3.45	2.31	33
3.0	3.39	2.23	34
2.2	1.32	1.41	−7
1.8	1	1	0